Characterization of poly(1,4-phenyleneterephthalamide) in concentrated sulphuric acid. 2: Determination of molecular weight distributions

Benjamin Chu
Departments of Chemistry and Materials Science and Engineering, State University of New York at Stony Brook, Long Island, New York, 11794-3400, USA

and Qicong Ying, Chi Wu, James R. Ford and Harbans S. Dhadal
Department of Chemistry, State University of New York at Stony Brook, Long Island, New York, 11794-3400, USA
(Received 7 June 1984)

By combining static and dynamic properties (M_w, A_2, k_d, R_g and R_h) of poly(1,4-phenyleneterephthalamide), PPTA (commercially known as Kevlar), with a detailed analysis of measured time correlation functions at different scattering angles in dilute solution, we have been able to estimate the molecular weight dependence of the radius of gyration, $R_g(M)$, the persistence length ρ (≈ 290 Å), and the molecular weight distribution (M_z:M_w:$M_n \approx 6.2$:1.8:1) using an *unfractionated* PPTA sample ($M_w = 4.3 \times 10^4$ g/mole). Laplace inversion of the time correlation function was accomplished independently by means of two different algorithms: the singular value decomposition technique with discrete multi-exponentials to approximate the normalized characteristic linewidth distribution function $G(\Gamma)$ and the method of regularization whereby a linearized smoothing operator was used. The non-intrusive laser light scattering technique permits us to characterize, for the first time, the molecular weight distribution of PPTA which has been difficult to perform by means of other more established methods, such as size exclusion chromatography, because of the corrosive nature of solvents used in preparing PPTA solutions.

(Keywords:

INTRODUCTION

In the previous paper, wa characterized the solution properties of poly(1,4-phenyleneterephthalamide), PPTA, in concentrated sulphuric acid (with and without the addition of a small amount of K_2SO_4) using light scattering intensity and linewidth measurements. We need the main result $\langle D \rangle_z \propto \bar{M}_w^{0.75}$ cm^2 s^{-1} with M_w expressed in [g/mole] in order to achieve an empirical transform from a distribution of translational diffusion coefficients to a molecular weight distribution. In this paper, the essential steps are to perform a Laplace inversion of the measured time correlation function and to take into account the effects of particle scattering, interaction and internal motions at finite scattering angles and concentrations so that we can obtain a simultaneous estimate of the persistence length and the molecular weight distribution. We used $k_D = 2.07 \times 10^{-5}$, instead of 2.11×10^{-5}, in the empirical relation $D_0 = k_D M^{-0.75}$ because of a possible difference in size for PPTA in 96% H_2SO_4 with and without K_2SO_4.

LAPLACE TRANSFORM

The instrumentation used in photon correlation spectroscopy (PCS) (or fast Fourier transform (FFT) spectral analysis) has gone through an era of considerable improvement, making it possible to accumulate auto-correlation (or power spectrum) profiles with extremely high signal to noise ratios. Consequently, we can obtain an accurate description of the distribution of characteristic decay times, Γ, which can be related to molecular parameters of interest.

In a self-beating experiment, under Gaussian conditions, the single-clipped photo-electron count auto-correlation function can be related to the first-order normalized electric field correlation function $g^{(1)}(\tau)$ by the Siegert relation

$$G_k^{(2)}(\tau) = N_s \langle n_k \rangle \langle n \rangle (1 + \beta |g^{(1)}(\tau)|^2) \qquad (1)$$

where $\langle n_k \rangle$ and $\langle n \rangle$ are the mean clipped and unclipped counts per sample time, N_s is the total number of samples, and k is the clipping level. The constant β accounts for the spatial averaging taking place at the detector and is normally treated as an unknown parameter to be determined by the analysis routines. The quantity $N_s \langle n \rangle \langle n_k \rangle [\equiv A]$ represents the baseline associated with the function $G_k^{(2)}(\tau)$. For scatters undergoing only Brownian motions the function $g^{(1)}(\tau)$ is related to the characteristic linewidth distribution $G(\Gamma)$ through a Laplace transform

$$g^{(1)}(\tau) = \int_0^\infty G(\Gamma) e^{-\Gamma\tau} d\Gamma \qquad (2)$$

The problem of correlation function profile analysis therefore consists of inverting the Laplace transform. The

* Author to whom requests for reprints should be addressed.

0032-3861/85/091408-11$03.00

more detailed procedures are presented because the inversion is an essential and crucial step in our data analysis.

From equation (1) we see that the *net* unnormalized electric field autocorrelation function, $(A\beta)^{1/2}g^{(1)}(\tau)=(G_k^{(2)}(\tau)-A)^{1/2}\equiv b_i$, is the experimental quantity of interest. We have found that in order to obtain a distortion-free $G(\Gamma)$ the quantity A must be known to within 0.2% and that errors greater than that will preclude meaningful analysis yielding no more than the average linewidth $\bar{\Gamma}$ and its variance $\mu_2/\bar{\Gamma}^2$ where $\mu_2=\int G(\Gamma)(\Gamma-\bar{\Gamma})^2 d\Gamma$.

Nature of the problem

Equation (2) is a Fredholm integral equation of the first kind and as such the associated inversion problem is notoriously ill-conditioned when the data are corrupted by noise. This inversion problem is endemic in the physical sciences and has received much attention in recent years[1-12]. The reader is advised to refer to specific topics in chapters of two recent books[10,11] dealing with linewidth polydispersity analysis for details. In the absence of systematic errors, noise becomes the sole obstacle to perfect restoration. Thus, for noisy data, the amount of information that can be retrieved may be severely limited. Any attempt to extract information beyond this limit may lead to physically unreal solutions. Correct inversion of equation (2) therefore must involve some means of restricting the amount of information that is sought; this can be done in the following ways:

(1) defining the problem in terms of a restricted set of information elements[2,12],

(2) using regularization techniques to seek smooth solutions[7],

(3) truncating the singular function expansion of the solution[9].

McWhirter and Pike[2], by decomposing the inversion problem of equation (2) in terms of the singular functions of the Laplace kernel, have shown that the maximum amount of information that can be recovered depends strongly on the level of noise in the data, and that in practice this information may be severely limited since the eigenvalues of the Laplace kernel fall below the level of noise very rapidly. Unfortunately a complete knowledge of the noise process is usually not available. Further improvements in restoring $G(\Gamma)$ can be achieved by the use of additional *a priori* knowledge of $G(\Gamma)$. The singular value decomposition technique[13-15] provides a means of determining the information elements of the actual problem (including constraints) and, by ordering these elements in decreasing importance, is a useful method which can estimate the amount of information retrievable for a given problem.

Regularization methods seek least squares minimization solutions to equation (2) subject to additional *a priori* constraints which restrict the set of possible solutions. These *a priori* constraints such as postivity prove useful in enhancing the known features of the distribution. One such scheme has been described elsewhere[16].

Singular value decomposition technique

In general, we seek solutions to equation (2) that minimize the L^2 norm of the discrepancies between the discretely sampled data points b_i and the corresponding values that would be calculated from our solution subject to the requirement that the solution be well behaved. The linear least squares minimization problem can be stated as

$$CP\simeq b \tag{3}$$

where P is the parameter vector of length n, C is the $(m\times n)$ curvature matrix, and b is the data vector of length m.m and n are respectively the number of data points in the net correlation function and the number of adjustable parameters of the model. The symbol $\simeq$ in equation (3) is intended to imply solution of the overdetermined set of equations subject to the least squares criterion (minimization of the Euclidean norm of the residual vector $\|b-CP\|$). The multiexponential method chooses a mathematically convenient form to approximate $G(\Gamma)$ that results in an overdetermined set of equations

$$G(\Gamma)=\sum_j P_j\delta(\Gamma-\Gamma_j) \tag{4}$$

This model leads to either a linear or nonlinear problem depending on whether or not the model for $G(\Gamma)$ is allowed to float in Γ-space. As the number of adjustable parameters increases, however, the problem rapidly becomes more susceptible to the ill-conditioning of equation (2), and one must be careful to include some form of rank reduction step in the analysis procedure. We have found the singular value decomposition technique quite helpful.

Substituting the model (equation (4)) into equation (2) gives

$$b_i=\sum_j P_j\exp(-\Gamma_j\tau_i) \tag{5}$$

The elements of C can be determined from a comparison of equations (2) and (4) with equation (3) to be

$$c_{ij}=e^{-\Gamma_j\tau_i} \tag{6}$$

where i and j are the row and column indices, respectively, and the parameters to be determined are the P_j, i.e. the weighting factors of the δ functions (see equation (4)).

In the multiexponential analysis we have used logarithmically spaced values of Γ representing the optimum spacing for sampling of functions of the exponential type[3]. In addition, it is important to keep in mind that although the output of the singular value decomposition algorithm can be a large number of parameters (typically 20), this does not mean that 20 *independent* parameters have been recovered from the data. Indeed, the P vector is reconstructed from a limited number (k, typically 3 or 4) of basis function.

Additional *a priori* constraints such as positivity can be introduced into the solution. Linear constraints can be incorporated as described in the section below on methods of regularization (see equation (26)). Implementation of nonlinear constraints such as positivity requires great care, as one should be aware of exactly how much improvement in the ill-conditioning has been effected.

Prescaling the columns of C to unit norm has been used to improve the numerical stability of the inversion (see for example, Lawson and Hanson (ref. 15, pp. 185–188). The scaling transforms equation (3) to

$$Ax \simeq b \tag{7}$$

where

$$A = CH \tag{8}$$

and

$$x = H^{-1}P \tag{9}$$

with H being a diagonal matrix whose nonzero elements are the reciprocals of the norms of the corresponding column of C,

$$h_{ij} = \left(\sum_i c_{ij}^2\right)^{-1/2} \delta_{ij} \tag{10}$$

The singular value decomposition consists of applying orthogonal transformations to the matrix A such that equation (7) becomes

$$USV^{-1}x = b \tag{11}$$

Here S is a diagonal matrix whose nonzero elements are the ordered singular values of the problem. Details of the algorithm may be found in Lawson and Hanson[15], as well as FORTRAN-IV code to implement the decomposition. Defining the new vectors y and g by

$$x = Vy \tag{12}$$

and

$$g = U^T b, \tag{13}$$

we have

$$Sy = g. \tag{14}$$

Since S is diagonal, we have immediately

$$y_i = g_i / s_{ii}. \tag{15}$$

It is at this point that the rank-reduction step is applied. The singular values s_{ii}, being the square roots of the eigenvalues of the matrix A^*A, are closely related to the information elements transmitted through the integral operator of equation (2). Those singular functions whose singular values are above the noise level should be included in the expansion of the solution vector. The problem is said to be of pseudorank k, k being the number of terms in the expansion. If k is known, we can compute the pseudoinverse of S, S^+, placing zeros in the locations of S^+ corresponding to those singular values buried in the noise. However, we do not usually know the experimental noise level, hence k is unknown. We therefore define a set of 'candidate solutions' $\{x^{(k)}\}$ from equation (12) as

$$x^{(k)} = Vy^{(k)} \tag{16}$$

where

$$y^{(k)} = \begin{cases} g_i/s_{ii} & \text{for } 1 \leqslant i \leqslant k \\ 0 & \text{for } k < i \leqslant n \end{cases} \tag{17}$$

From equation (9) we have a set of candidate solutions for the original P vector of equation (3) defined by

$$P^{(k)} = Hx^{(k)} \tag{18}$$

with a corresponding set of residual vectors $\{r^{(k)}\}$ such that

$$r^{(k)} = CP^{(k)} - b \tag{19}$$

There are several criteria for the selection of the particular value of k that can be applied (see chapters 25 and 26 of Lawson and Hanson[15]). One that we have found useful is to examine a plot of $\ln\|r^{(k)}\|$ vs. $\ln\|P^{(k)}\|$. We endeavour to select k such that $\|r^{(k)}\|$ is 'sufficiently small' without $\|P^{(k)}\|$ getting 'too large'. This is directly analogous to the 'energy' constraint of some regularization methods.

Methods of regularization

Equation (2) belongs to the general class of linear Fredholm integral equations of the first kind

$$\bar{b}(\tau) = \int_{\Gamma_{\min}}^{\Gamma_{\max}} K(\tau, \Gamma) G(\Gamma)\, d\Gamma, \qquad 0 < \tau < \infty \tag{20}$$

where $G(\Gamma)$ is the distribution function to be determined, $K(\tau, \Gamma)$ is a general kernel which in the case of the Laplace transform is given by $e^{-\Gamma\tau}$, and $\bar{b}(\tau)$ is the noise free data function. We present the method in terms of continuous functions; extension to the discrete case is straightforward and discussed in Chu *et al.*[17]. The regularization methods impose stability on the solution by the use of reasonable constraints and have been the subject of many studies[18-22]. The original problem is transformed into one possessing the desired properties. It should be noted that this method is not the only means of restoring stability to the ill-posed problem. For example, one may regularize such a problem by changing the definition of what is meant by ill-posed. A discussion of this is given by Nashed[22].

Abbiss *et al.*[23] used the methods of Tikhonov and Miller[18,19] to derive iterative and non-iterative regularized solutions for the inversion of a similar equation which arises in Fourier optics and in the extrapolation of band-limited signals. Following the steps outlined in Abbiss *et al.*[23] we introduce the function $r(\tau)$ to account for the perturbation to the data (e.g. additive noise). Equation (20) becomes

$$b(\tau)[=\bar{b}(\tau)+r(\tau)] = \int_{\Gamma_{\min}}^{\Gamma_{\max}} K(\tau, \Gamma) G(\Gamma)\, d\Gamma + r(\tau) \tag{21}$$

or, in operator form,

$$b = KG + r \tag{22}$$

In the absence of *a priori* knowledge of $r(\tau)$ one might attempt to solve the problem

$$b = K\phi \tag{23}$$

for the distribution ϕ, assuming this to be 'close to', in some sense, the true distribution G. Indeed, the singular value technique described previously takes this approach. However, one must be careful to account for the ill-posedness of the problem, as the solution ϕ is extremely sensitive to small perturbations in b. The rank reduction step of the singular value decomposition approach is crucial to restricting this sensitivity; without it the solution ϕ may bear no resemblance to the true distribution G. The regularization technique solves a related equation whose solution responds stably to perturbations in the data and yet is constrained to be close to the true distribution G.

Following Abbiss *et al.*[23] we minimize the following functional:

$$F(u) = \|b - Ku\|^2 + \alpha\|Cu\|^2 \tag{24}$$

where u represents the possible set of functions satisfying equation (24), α is a small positive quantity referred to as the regularization parameter, C is a linear constraint operator with a bounded inverse, and $\|h\|$ denotes the L^2

norm of $h(x)$ on $[x_1, x_2]$

$$\|h\|^2 = \int_{x_2}^{x_1} |h(x)|^2 \, dx \tag{25}$$

We assume G and b to be square integrable function on $[\Gamma_{min}, \Gamma_{max}]$ and on $[0, \infty]$ respectively. Taking C to be the identity operator, it is apparent that equation (24) represents the minimization of the residual norm $\|b - Ku\|$ subject to the condition that the norm of the solution $\|u\|$ be finite. Additional *a priori* knowledge may be incorporated by suitable choice of C. By the application of variational calculus[24] the minimum of equation (24) can be shown to occur for that estimate $\tilde{G}$ which is the solution of the equation

$$[K^*K + \alpha C^*C]\tilde{G} = K^*b \tag{26}$$

where the * denotes the adjoint operator[25]. We describe an iterative means of solving equation (26) that allows incorporation of the (nonlinear) positivity constraint. Rewriting equation (26) in the form $\tilde{G} = \tilde{G} + K^*b - [K^*K + \alpha C^*C]\tilde{G}$ suggests the iterative scheme,

$$\tilde{G}^{(N)} = K^*b + [(1-\alpha)I - K^*K]\tilde{G}^{(N-1)} \tag{27}$$

where we have taken C to be the identity operator, I. The notation $\tilde{G}^{(N)}$ represents the N^{th} iteration estimate of $\tilde{G}$. The convergence of equation (27) is guaranteed if the norm of the operator $[(1-\alpha)I - K^*K]$ is strictly bounded by unity for all $\alpha < 1$. Using the singular values of the Laplacian kernel computed by Bertero *et al.*[12], it can be shown that equation (27) in the limit of infinite iterations converges to the solution of equation (26). At this point, it should be noted that the convergence of an iterative sequence to a well-behaved solution, by itself, is not a sufficient condition to establish regularization. One must show that the solution $\tilde{G}$ tends to the true distribution G as the noise on the data tends to zero. Chu *et al.*[17] establish this convergence by presenting a singular function decomposition of the solution. It is also shown that the number of iterations N can be used to restrict the unregularized ($\alpha = 0$) solution to a finite set of singular values, analogous to the rank reduction step of the singular value decomposition method.

In the case of the Laplace inversion, we have

$$(KG)(\tau) = \int_{\Gamma_{min}}^{\Gamma_{max}} e^{-\Gamma\tau} G(\Gamma) \, d\Gamma, \qquad 0 < \tau < \infty \tag{28}$$

$$(K^*b)(\Gamma) = \int_0^{\infty} e^{-\Gamma\tau} b(\tau) \, d\tau, \qquad \Gamma_{min} < \Gamma < \Gamma_{max} \tag{29}$$

Therefore,

$$(K^*KG)(\Gamma) = \int_0^{\infty} e^{-\Gamma\tau} \, d\tau \int_{\Gamma_{min}}^{\Gamma_{max}} e^{-z\tau} G(z) \, dz$$

By changing the order of integration we find

$$(K^*KG)(\Gamma) = \int_{\Gamma_{min}}^{\Gamma_{max}} \frac{1}{\Gamma + z} G(z) \, dz$$

In the analysis of real data, the measurement of $b(\tau)$ will be confined to $\tau_{min} < \tau < \tau_{max}$. Equation (29) becomes

$$(K^*b)(\Gamma) = \int_{\tau_{min}}^{\tau_{max}} e^{-\Gamma\tau} b(\tau) \, d\tau, \qquad \Gamma_{min} < \Gamma < \Gamma_{max} \tag{30}$$

Therefore,

$$(K^*KG)(\Gamma) = \int_{\Gamma_{min}}^{\Gamma_{max}} \frac{e^{-\tau_{min}(\Gamma+z)} - e^{-\tau_{max}(\Gamma+z)}}{(\Gamma+z)} G(z) \, dz \tag{31}$$

Equations (27), (30) and (31) can be used to implement the iterative scheme for recovering the characteristic linewidth distribution function from the experimental data. The iterative sequence in equation (27) is used to estimate the Nth approximation to $G(\Gamma)$. The initial estimate $\tilde{G}^{(0)}$ can be taken to be $(K^*b)(\Gamma)$; alternatively one may use estimates obtained from other techniques such as the singular value decomposition approach. The choice of α, Γ_{min} and Γ_{max} is straightforward and can be achieved in an automated procedure without user interaction. The regularization parameter is a function of the level of noise in the data, that is, $\alpha = \varepsilon^{\rho}$ with $\rho < 1$. Predicting the optimum choice of α, assuming one exists, requires knowledge of the characteristics of the linewidth distribution to be recovered as well as that of the noise process. When close to unity, α has the effect of completely suppressing noise but unfortunately at the expense of smoothing the characteristic linewidth distribution to be recovered. Values close to zero allow the propagation of noise through the solution. A sufficient guideline is that α be as close to zero as possible in order to allow the maximum amount of information to be retrieved from the data while still retaining the stability of the solution. Fisher's statistic test has been used in another regularized scheme[16] for determining the optimum solution.

A PRACTICAL PROCEDURE FOR CORRELATION FUNCTION PROFILE ANALYSIS

Baseline considerations

In the previous discussion, we have noted that estimates on $G(\Gamma)$ are accessible if we have very precise time correlation function data and know the limitation of Laplace inversion due to its ill-conditioned nature. Experimentally, our measurements were always performed at finite concentrations and scattering angles. Therefore, in order to determine a representative distribution of translational diffusion coefficients where $\Gamma_j = D_j K^2$ with j being a representative component, we needed to extrapolate a distribution of characteristic decay times $G(\Gamma)$ to 'zero' scattering angle and zero concentration. As the $G(\Gamma)$ distributions were estimates, we used the same inversion procedure so as to reduce systematic error differences. Furthermore, based on physical arguments, we took the PPTA molecular weight distribution to have both low and high molecular weight cut-offs, even though we do not know the exact cut-off values. For example, it is reasonable to assume that the molecular weight of PPTA must be greater than that of its monomer. We have, however, not set an upper bound because of possible aggregation in PPTA solutions. Nevertheless, for PPTA samples in Part 1 with $1.4 \times 10^4 < M_w < 4.8 \times 10^4$ g/mole, there must be an upper bound in the molecular weight distributions. In order to determine the upper and lower bounds of $G(K, \Gamma)$ in a systematic way, we have added a constraint to the equation

$$G(K, \Gamma) = \sum_j P_j(K) \delta(\Gamma - \Gamma_j) \tag{32}$$

such that the ratios of $G(\Gamma_1)/G(\Gamma_2)$ and $G(\Gamma_N)/G(\Gamma_{N-1})$ are about 1%, signifying well defined values of $\Gamma_{max}(\sim\Gamma_N)$ and $\Gamma_{min}(\sim\Gamma_1)$. It should be noted that we have not made precise determinations of Γ_{max} and Γ_{min} whose values are governed by the ill-considered nature of the Laplace transform. Rather, we aim to determine a consistent set of Γ_{min} and Γ_{max} values of $G(\Gamma)$ over a range of scattering angles. The 1% criterion is also not important as shall be demonstrated later. Introduction of this *a priori* knowledge permits us to relax requirements for agreement between the measured baseline, $A\beta|g^{(1)}(\tau\rightarrow\infty)|^2$, and the computed baseline, $N_s\langle n_k\rangle\langle n\rangle$. In other words, if we observed a disagreement between measured and computed baseline of the order of a few tenths of one percent, say 0.2%, we cannot only accept such data but also permit baseline adjustments within the statistical error limits ($\sim$0.1%) so long as the resultant $G(\Gamma)$ satisfies our *a priori* knowledge on the form of the characteristic decay time distribution. Such a relaxation in the constraint of the precision required in measured data can lead to serious errors without a proper understanding of the ill-conditioned problem in the Laplace transform. What we have claimed is not that our correlation function profile analysis requires a floating baseline in order to achieve the desired results, but that from physical arguments, we know our measured data to contain small (within statistical error limits of the baseline) amounts of large particles which have not been removed by standard solution clarification procedures. The presence of a trace amount of such large particles interferes with our data analysis. We claim that we can still make use of slightly imperfect data if the amount of such large particles present is very small, so small that its contribution to the time correlation function falls within the statistical error limits of our baseline measurements. If we were to clarify our polymer solutions more carefully, we can obtain identical results in $G(\Gamma)$ without floating the baseline. Indeed, subsequent tests show that the above procedure is appropriate. The reasons we want to emphasize the importance of baseline measurements and at the same time the justification of a small amount of baseline adjustments which are not more than the order of magnitude of statistical fluctuations of our baseline measurements, i.e., $\lesssim$0.2%, are that we then have a larger data set available for our analysis and that we no longer need to be so very careful so as to accept only those measured correlation functions whose measured and computed baselines agree to within $\sim$0.1%. A further test on acceptance of a slight baseline adjustment is that, for a given PPTA solution, the baseline adjustment must decrease rapidly with increasing scattering angle since intensity contributions from such large particles are important at relatively small scattering angles. In most cases, we adjust no more than 0.1% of the measured baseline value in order to test its effects on the characteristic decay time distribution function $G(\Gamma)$. In the following typical analysis, we demonstrate our procedure first using the multiexponential (equation (5)) singular value decomposition method and then the method of regularization.

The *Figure 1a* shows an experimental net unnormalized electric field autocorrelation function, electric field autocorrelation function, $b_i \equiv b(\tau)=[G_k^{(2)}(\tau)-A]^{1/2}=[A\beta|g^{(1)}(\tau)|^2]^{1/2}$, for a PPTA ($M_w=4.3\times10^4$ g/mole) sample dissolved in 96% H_2SO_4 and 0.05 M K_2SO_4 and measured at $C=2.8\times10^{-4}$ g/ml, $\theta=45°$, and 30°C. The 91-decay channel ($i=2,92$) single-clipped net time correlation function (with delay time increments of 190 μs each) show some fluctuations and suggest the quality of data needed to perform a more detailed correlation function profile analysis. *Figure 1b* shows the relative deviation of the discrete time correlation function, $[b_i-b_i$ (equation (5))$]/b_i$, where the computed b_i based on

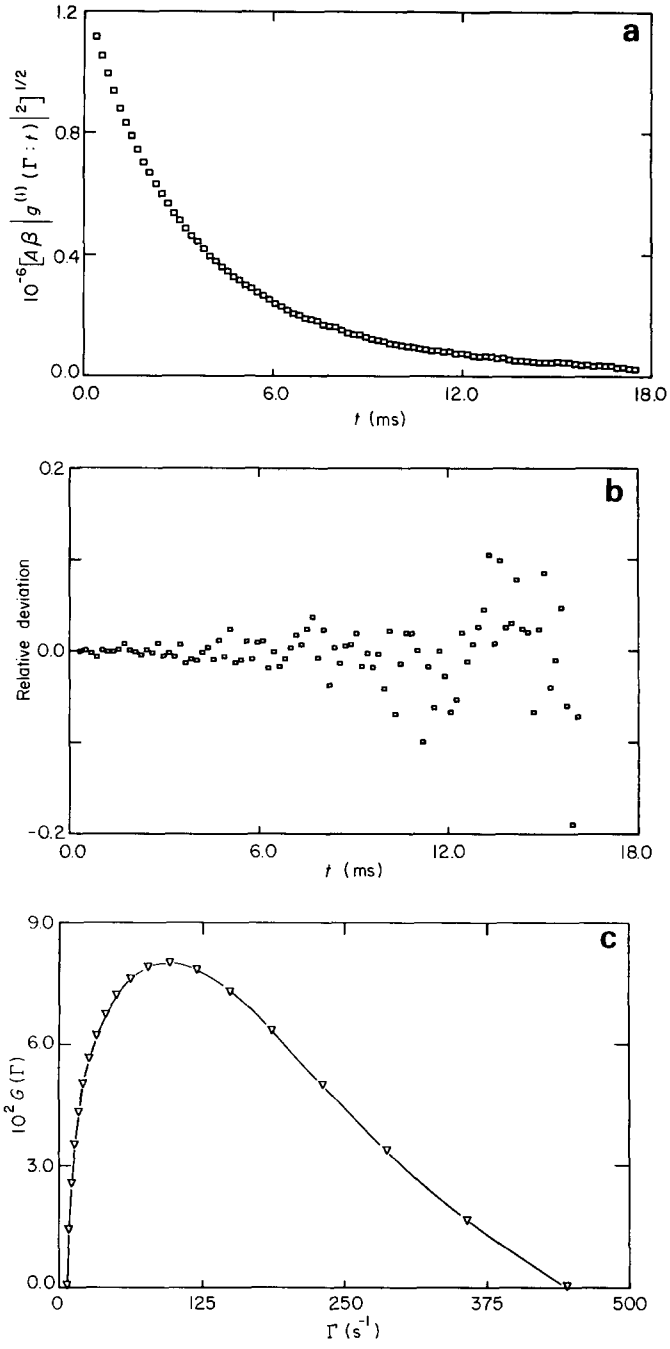

Figure 1 (a): A typical net unnormalized electric field autocorrelation function. 2.8×10^{-4} g/ml PPTA ($M_w=4.3\times10^4$ g/mole) in 96% H_2SO_4 and 0.05 M K_2SO_4 measured at $\theta=45°$ and 30°C using $\Delta\tau=190\,\mu$s. (b): A relative deviation plot of measured and computed (from equation (5)) time correlation function. (c): Characteristic linewidth distribution for *Figure 1a*). (△) represent the location of the δ-functions used according to the multiexponential model: $G(\Gamma_j)=\sum_j P_j\delta(\Gamma-\Gamma_j)$ by means of the singular value decomposition algorithm. The height of each hollow triangle has been rescaled according to P_j/Γ_j in order to account for the unequal spacing of the δ-functions. $G(\Gamma)$ as presented is a continuous distribution function

equation (5) uses a $G(\Gamma)$ distribution, as shown in *Figure 1c* which was obtained by means of the singular value decomposition technique. In *Figure 1c*, we note that $G(\Gamma)$ has 20 unequally-spaced representative elements [$j = 1,20$ in equation (5)] and the P vector is reconstructed from $k = 3$ basis functions. Furthermore, the hollow triangles representing the locations of the δ functions in the Γ-axis have P_j/Γ_j values, not P_j values, along the $G(\Gamma)$ axis so that a continuous distribution of $G(\Gamma)$ can be presented from $G(\Gamma_j) = \sum P_j \delta(\Gamma - \Gamma_j)$ where the discrete Γ_j's are not spaced linearly. The procedure for choosing the correct number of parameters is illustrated in *Figure 2a*, which shows a sequence of solutions for $k = 2, 3, 4$ together with a plot of $\ln\|r^{(k)}\| (\equiv W)$ vs. $\ln\|P^{(k)}\| (\equiv Z)$. Note that $k = 3$ satisfies our criterion for the best solution. *Figure 2b* shows a series of solutions obtained using the method of regularization, equation (27), for various values of α ($\alpha = 0$, 0.0003, 0.001). We choose the smallest value of α so that the solution is well behaved at the end points.

Change of variables

From the previous section (Baseline considerations), we showed that we can determine $G(\Gamma)$ in the time correlation function measured at finite concentration and finite scattering angle. If $\Gamma = DK^2$, we can easily transform $G(\Gamma)$ to $G(D = \Gamma/K^2)$ at the same finite concentration.

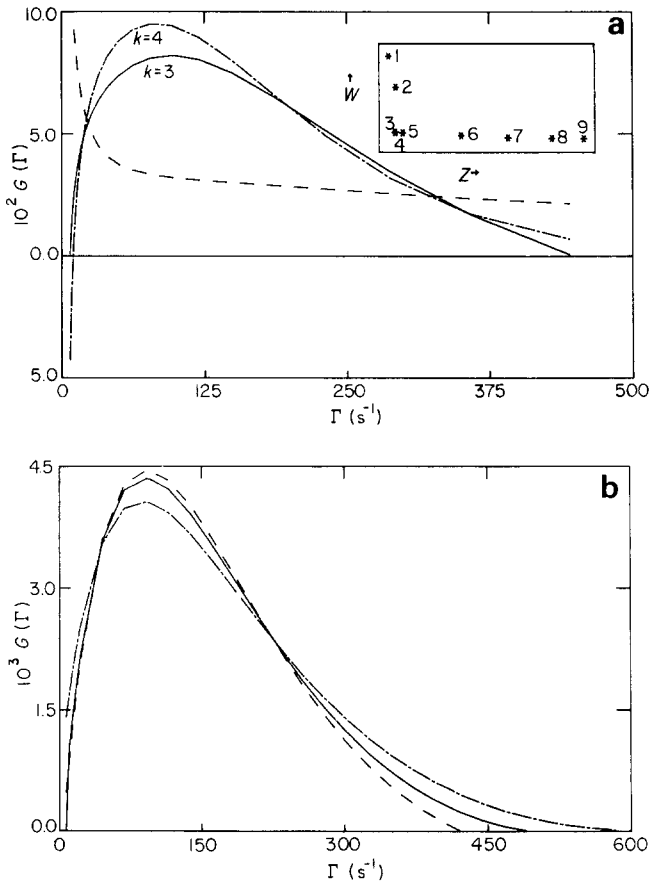

Figure 2 (a): Singular value decomposition analysis of the data in the upper curve of *Figure 1*. Three candidate solutions for $k = 2$, 3 and 4 are shown together with a plot of $\ln\|r^{(k)}\| (\equiv W)$ vs. $\ln\|P^{(k)}\| (\equiv Z)$ showing why $k = 3$ is selected as the best possible solution. Numbers in the inset refer to k values. (b) Regularized solution to equation (2), for the data in *Figure 1a*. Solution for various values of α (solid: $\alpha = 0.0003$, broken: $\alpha = 0$ and dashed-dot: $\alpha = 0.001$) show the over smoothing that can arise if α is large. All the regularized solutions have been forced to be positive

However, for worm-like chains, polymer molecules of even modest molecular weights have fairly large radii of gyration so that the condition $KR_g < 1$ is not easily satisfied. We need to devise an approach to extrapolate $G(\Gamma)$ to sufficiently low scattering angles so that the condition $D = \Gamma/K^2$ is satisfied.

Stockmayer and Schmidt[26] considered the effects of chain stiffness, branching and polydispersity and expressed the characteristic decay time in powers of K^2:

$$\Gamma = DK^2(1 + fR_g^2K^2) \tag{33}$$

where the first-term has the standard K^2 dependence due to the translational motions of the centre of mass of polymer molecules. At low K, $\Gamma = DK^2$. As K is increased, we have an effective increase in the average characteristic decay time due to internal molecular motions. The second term is proportional to K^4 and depends upon molecular size, being proportional to the square of radius of gyration R_g^2. f is a dimensionless number that in general depends on chain structure, polydispersity and solvent power.

At a fixed scattering angle, we know that the total intensity scattered by all the species in the scattering volume must be equal to the integrated scattered intensity at the same scattering angle. Thus, if we have representative fractions, $\sum_{j=i} P_j(K)$ is proportional to the excess scattered intensity at K. For a set of $G(K, \Gamma)$ distributions measured at a finite concentration, we can scale $\int G(K, \Gamma)\,d\Gamma$ according to the Rayleigh ratio $R_{vv}(K)$ as shown in *Figure 3*. In view of the fact that there are uncertainties associated with the Laplace inversion, we need to establish a procedure to identify the corresponding representative fractions at different scattering angles. As the initial lineup, we shall use the relation $\bar{\Gamma} = D_z K^2(1 + fR_{g,app}^2K^2)$ where $\bar{\Gamma} (\equiv \int \Gamma G(\Gamma)\,d\Gamma)$ is the average linewidth. The other discrete representative fractions follow arbitrary linear steps towards left and right of $\bar{\Gamma}$ according to $(\bar{\Gamma} - \Gamma_{min})/n$ and $(\bar{\Gamma}_{max} - \Gamma)/m$ with n and m being the *arbitrary* number of representative fractions which we wish to construct. It should be noted that we have two extrapolations which we are making:

(1) Along the Γ-axis, we use the relation $D^* = \Gamma/K^2 = ((1 + fR_{g,app}^2K^2)$. In a plot of D^* *versus* K^2 for different representative fractions as shown typically in *Figure 4*, we can compute D and $fR_{g,app}^2$ for the representative fractions.

(2) Along the $G(\Gamma)$ [or $G^+(D^*)$] axis, we can compute $R_{g,app}^2$ from plots of $1/G^+(D^*)$ *versus* K^2 as shown typically in *Figure 5*. The superscript + denotes unnormalized distribution.

At finite concentrations, the Rayleigh ratio for worm-like chains with molecular anisotropy δ has the approximate form:

$$\frac{HC}{R_{vv}} = \frac{1}{M_{app}}\left(1 + \frac{R_{g,app}^2K^2}{3} + \ldots + \frac{2A_2C}{(1 + 4/5\delta^2)}\right) \tag{34}$$

where

$$M_{app} = (1 + 4/5\delta^2)M_w \tag{35}$$

$$R_{g,app}^2 = \frac{(1 + 4\delta/5 + 4\delta^2/7)}{1 + 4\delta^2/5} R_g^2(C) \tag{36}$$

Equations (35) and (36) correspond to equations (6) and (8) of Paper 1. By combining corrections for molecular anisotropy and finite concentration, we finally get

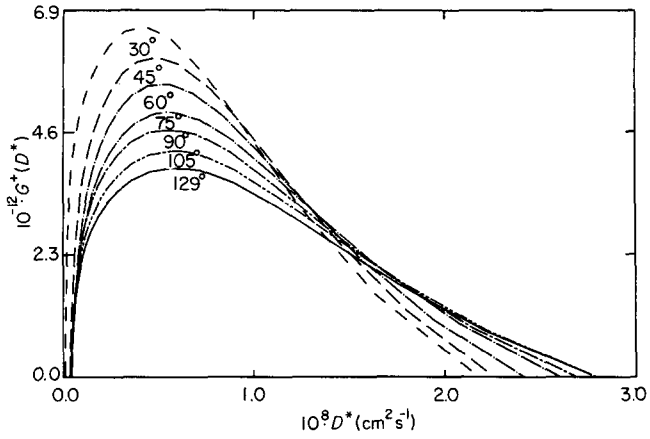

Figure 3 Plots of $G^+(D^*)$ *versus* D^* for PPTA ($M_w = 4.3 \times 10^4$ g/mole) in 96% H_2SO_4 and 0.05 M K_2SO_4 measured at 30°C with θ varying from 30° to 129°. $\int G(D^*)dD^*$ has been scaled according to the angular distribution of excess integrated scattered intensity based on equations (1) and (7) of Paper I and values of R_g, δ, M_w and A_2 values in *Table 1* of Paper I. $D^* = \Gamma/K^2 = D(1 + fR_{ga}^2K^2)$ where R_{ga} is the apparent radius of gyration at finite concentration

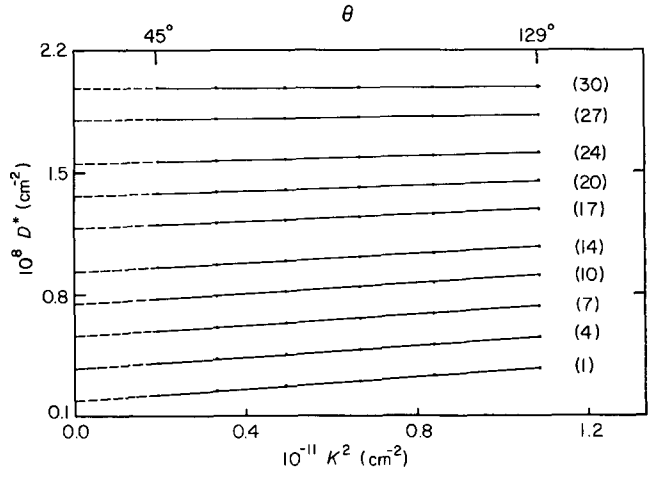

Figure 4 Plots of D^* *versus* K^2 based on results of *Figure 3*. Some numerical values are tabulated in *Table 1*

$$R_g^2(0) = R_g^2(C)\left(1 + \frac{2A_2M_wC}{(1+4/5\delta^2)}\right) \quad (37)$$

From equation (34), we can retrieve equations (7) and (9) of Paper 1 by extrapolation to $C=0$ and $\delta=0$, respectively. The above equations are the fundamental relations in light scattering intensity measurements which we need to connect with the light scattering characteristic decay time distribution when we change $G(\Gamma)$ *versus* Γ, as shown in *Figure 1c*, to $G(D^*)$ *versus* D^*, as shown in *Figure 3*.

At infinite dilution, we have for a continuous distribution

$$\int G(K,\Gamma)d\Gamma = \int G(K,\Gamma)K^2 d(\Gamma/K^2) = \int G(D^*)dD^* \quad (38)$$

where $D^* = \Gamma/K^2 = D_0(1 + fR_{g,app}^2K^2)$ and $G(D^*) = G(K,\Gamma)K^2$. By equating $\int G^+(K,\Gamma)d\Gamma$ with $R_{vv}(K)$, we take into account the integrated intensity scattered by all molecular species since at infinite dilution

$$R_{vv}(K) \sim \int F_n(M)M^2P(K)dM \quad (39)$$

where $F_n(M)$ and $P(K)$ are the number distribution and the particle scattering factor. The $\sim$ sign denotes that we are not concerned with the proportionality constant and that we have assumed the molecular anisotropy to be independent of molecular weight. According to the empirical relation $D_0 = k_DM^{-a}D$ and equations (38), we have

$$dD^* = -k_D\alpha_DM^{-(\alpha_D+1)}(1 + fR_{g,app}^2K^2)dM \quad (40)$$

Thus,

$$\int G^+(D^*)dD^* \sim \int \frac{P(K)}{(1 + fR_{g,app}^2K^2)}dD^* \quad (41)$$

or

$$1/G^+(D^*) \sim \frac{1 + fR_{g,app}^2K^2}{P(K)}$$
$$\sim 1 + (f + 1/3)R_{g,app}^2K^2 + O(K^4) \quad (42)$$

where the superscript + is introduced to emphasize that the scaled characteristic diffusion coefficient distribution is no longer normalized. By combining equations (33) and

Table 1 Numerical values of arbitrary representative fractions of a PPTA solution based on *Figures 1–5*

Fraction No.	D (10^{-8} cm^2 s^{-1})	M (10^4 g/mole)	R_{ga}^2 (10^{-11} cm^2)[a]	R_g^2 (10^{-11} cm^2)[b]	f
4	0.305	13.2	2.7	3.5	0.23
5	0.375	10.0	2.2	2.8	0.22
6	0.444	7.98	1.8	2.4	0.22
7	0.514	6.57	1.6	2.1	0.22
8	0.584	5.55	1.5	1.9	0.21
9	0.653	4.77	1.3	1.7	0.21
10	0.723	4.17	1.2	1.5	0.20
11	0.793	3.69	1.0	1.3	0.20
12	0.863	3.29	0.92	1.2	0.20
13	0.934	2.97	0.82	1.1	0.19
14	1.00	2.69	0.72	0.93	0.19
15	1.07	2.46	0.65	0.84	0.19
16	1.14	2.26	0.56	0.73	0.19
17	1.21	2.09	0.50	0.64	0.19
18	1.28	1.94	0.44	0.57	0.19
19	1.35	1.81	0.39	0.50	0.19
20	1.43	1.69	0.34	0.44	0.19

[a] R_{ga} is the apparent radius of gyration at finite concentration without correction for molecular anisotropy
[b] R_g is the radius of gyration at infinite dilution after correction for molecular anisotropy

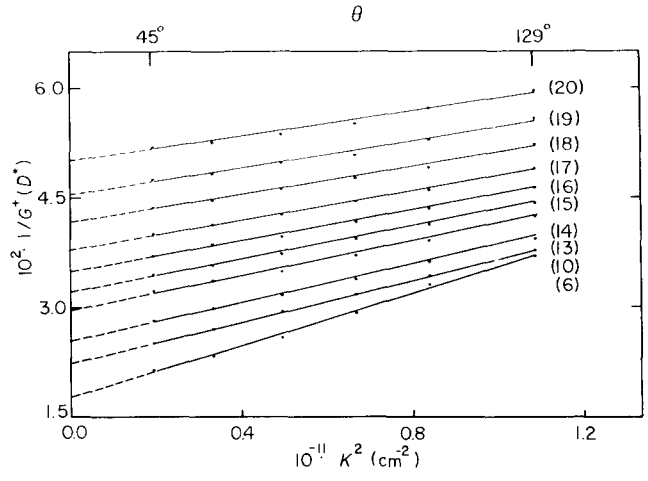

Figure 5 Plots of $1/G^+(D^*)$ *versus* K^2 based on results of *Figure 3*. Some numerical values are tabulated in *Table 1*

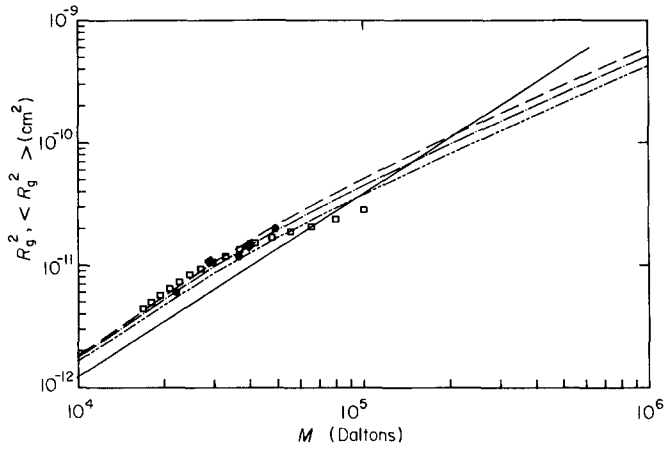

Figure 6 Plot of R_g^2 *versus* M based on values of R_{ga}^2 listed in *Table 1* with $R_g^2(0)=[1+2A_2MC/(1+\delta^2/5)][(1+4\delta^2/5)/(1-4\delta/5+4\delta^2/7)]R_{g,app}^2$. Solid line denotes $R_g^2=1.22\times10^{-18}M^{1.5}$ cm² with M expressed in g/mole. If we take $R_g^2=\rho^2\{4\rho/3-1+2/(L/\rho)-[2/(L/\rho)^2](1-\exp(-(L/\rho))\}$ where $L=12.9M/238$ with M expressed in [g/mole], we note that (– · · –)$\rho=240$ Å, (– · –)$\rho=290$ Å, (——)$\rho=340$ Å. From the $G(\Gamma)$ distribution function, R_g^2 values are more reliable in the higher characteristic frequency regime because of shallower slopes in *Figure 3*. Thus, we *estimate* $\rho\sim290$ Å. $\langle R_g^2\rangle_z$ values from light scattering intensity measurements are also presented as solid circles. It should be noted that R_g^2 values from *Table 1*, as denoted by hollow squares, are those of representative monodisperse fractions in a polydisperse sample while $\langle R_g^2$, as denoted by filled symbols, are z-average values of polydisperse samples. Filled circles denote PPTA in 96% H_2SO_4; filled diamonds, PPTA in 96% H_2SO_4

(42), we can determine both f and $R_{g,app}^2$. We have been able to determine f for different representative molecular weight fractions of PPTA within the polydisperse sample at finite concentrations as listed in *Table 1*.

From *Table 1*, if we take $R_{g,app}^2=1.3\times10^{-11}$ cm² for fraction 9 where $M=4.8\times10^4$ g/mole and $\delta\cong0.2$, we can compute $R_g^{*2}(C)\simeq[(1+4\delta^2/5)/(1-4\delta/5+4\delta^2/7)]R_{g,app}^2=1.55\times10^{-11}$ cm² (or $R_g^*=39$ nm at $C=2.8\times10^{-4}$ g/ml) or $R_g(0)=R_g^*(C)[1+2A_2MC/(1+4\delta^2/5)]^{1/2}\simeq41$ nm, which is in reasonable agreement with values listed in *Table 1* of Paper I. *Figure 6* shows a plot of R_g^2 *versus* M based on values of $R_{g,app}^2$ listed in *Table 1*. In the plot we have corrected $R_{g,app}^2$ to the radius of gyration R_g^2 at infinite dilution. If we take $\alpha_D=0.75$, $R_g^2=k_RM^{1.5}$ as shown by the solid line (——) in *Figure 6*. However, over the molecular weight range of the polydisperse PPTA sample ($M_w=4.3\times10^4$ g/mole), the worm-like chains behave more like rods at lower molecular weight fractions but become more coil-like at higher molecular weights. Therefore, no single exponent can closely depict $R_g(M)$ behaviour, as shown typically by the dashed curve for worm-like chains with a persistence length of 290 ± 50 Å.

Figure 7 shows a plot of f *versus* L/Λ with L and Λ being the contour length and the Kuhn length, respectively. We have taken $L=12.9$ $M/238$ Å and $\Lambda=2\rho=580$ Å. The values of f which we have determined are those from representative fractions of our polydisperse PPTA sample without actual fractionation. Its agreement with estimates predicted by Stockmayer and Schmidt[26,27] is amazing. We do not claim its precision to warrant a test on the form of f as a function of L/Λ at this time. Nevertheless, the result illustrates such a possibility and lends confidence to the procedure we have devised in extrapolating $G(\Gamma)$ to $G(D)$. It should also be emphasized that we have actually

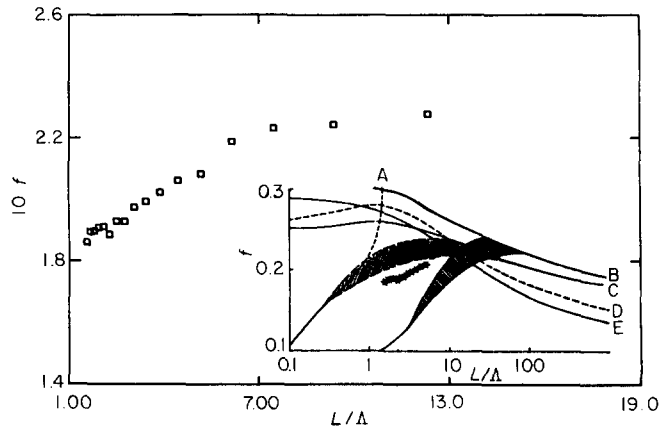

Figure 7 Plot of f *versus* L/Λ where L and Λ are the contour length and the Kuhn length, respectively. $L=12.9M/238$[Å] with M expressed in [g/mole]. $\Lambda=2\rho\simeq580$ Å with ρ taken to be 290 Å. Insert represents *Figure 3* of Stockmayer and Schmidt[26] (upper curve) for various approximate models of worm-like chains and curve A in *Figure 2* of a recent paper by Schmidt and Stockmayer[27] (lower curve). Notations A, C, D, E correspond to $P\theta_H$, AGK_n, AGK_p, HBH in *Figure 3* of ref. 26. B corresponds to a portion of A in *Figure 2* of ref. 27. The stars denote the measured f (at finite concentrations)

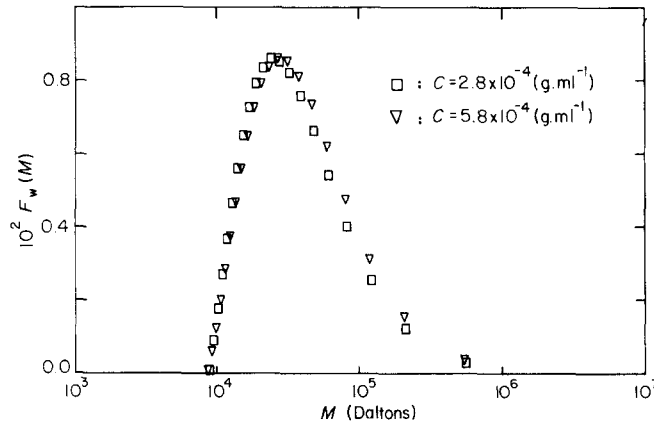

Figure 8 Molecular weight distribution of PPTA ($M_w=4.3\times10^4$ g/mole) using the method of regularization. $F_w(M)$ denotes the weight distribution

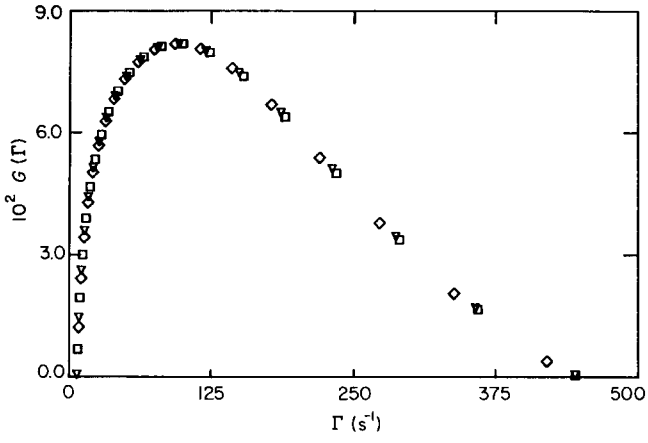

Figure 9 Plots of $G(\Gamma)$ *versus* Γ for the same data as in *Figure 1*. Variations of Γ_{min} and Γ_{max} have been introduced to examine the form of $G(\Gamma)$. Note Γ_{min} and Γ_{max} refer to the lowest and highest values of Γ used in the multiexponential model, not the location where $G(\Gamma)$ becomes 0. ▽: $\Gamma_{min}=7.0\,s^{-1}$; $\Gamma_{max}=445\,s^{-1}$; $\bar{\Gamma}=160.9\,s^{-1}$; □: $\Gamma_{min}=7.7\,s^{-1}$; $\Gamma_{max}=445\,s^{-1}$; $\bar{\Gamma}=160.9\,s^{-1}$; ◇: $\Gamma_{min}=7.7\,s^{-1}$; $\Gamma_{max}=420\,s^{-1}$; $\bar{\Gamma}=161.3\,s^{-1}$

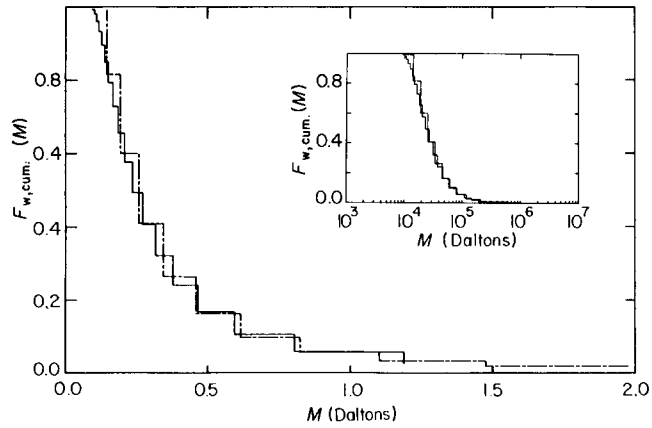

Figure 10 Integrated molecular weight distribution of PPTA based on *MWD* shown in *Figure 11*. Inset represents a plot of $F_{w,cum}(M)$ *versus* $\log M$. Singular value decomposition ——— corresponding to □ in *Figure 11*. Regularization —— corresponding to ▽ in *Figure 11*. $F_{w,cum}(M)=\int_{\infty}^{M} F_w(M)\,dM/\int_{\infty}^{0} F_w(M)\,dM$

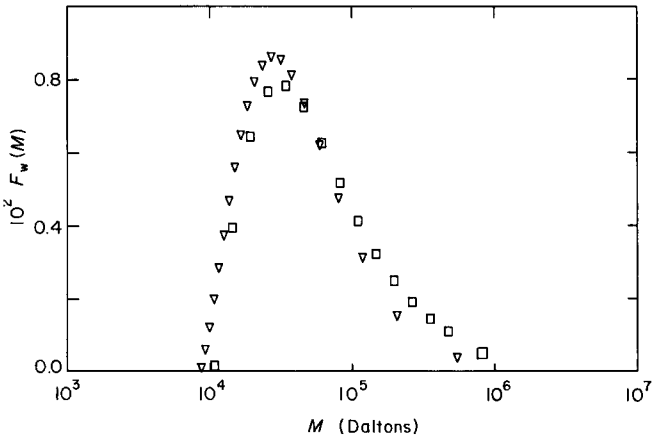

Figure 11 Molecular weight distributions of the same PPTA solution using two different methods ('singular value decomposition technique' and 'methods of regularization'). Hollow squares denote multi-exponential singular value decomposition method. Inverted hollow triangles denote method of regularization. The two distributions exhibit similar $M_z:M_w:M_n$ ratios. A small high molecular weight tail remains

determined some effective values of f at a finite concentration. The f values should decrease with decreasing concentration. We plan to discuss this point in a future publication. In the insert of *Figure 7*, we have plotted our measured f (at finite concentration) as stars in Figure 3 of Stockmayer and Schmidt[26] and in Figure 2 of Schmidt and Stockmayer[27] for various approximate models of semiflexible chains. The shaded areas represent their estimate of the correct curve. The agreement in the trend, and even in the magnitude, is remarkable. Our apparent values appear to be in closer agreement with the earlier 'polydisperse' curve, while $f(C\rightarrow 0)$ should in fact agree more closely with their later estimates, without even worrying about the molecular diameter.

In order to compute the translational diffusion coefficient at infinite dilution, we have estimated the concentration effect to be relatively small with $D=D_0(1+60C)$ with C expressed in [g/ml]. Thus, at $C=6\times 10^{-4}$ g/ml the correction term corresponds to less than 4% . It is, therefore, certainly appropriate to assume the diffusion second virial coefficient to be independent of molecular weight for this correction. By using the extrapolated $(K\rightarrow 0)$ values of $G^+(D^*)$ from *Figure 5* and of D_0 from *Figure 4* and the concentration correction, we have obtained a tramslational diffusion coefficient distribution function in the absence of interactions and intramolecular interference effect.

Molecular weight distribution

Having computed $G^+(D_0)$ at infinite dilution and 'zero' scattering angle, we can make use of the empirical relation $D_0=k_D M^{-0.75}$ from Paper I and determine the molecular weight distribution. Again, it should be noted that the exponent $\alpha_D=0.75$ represents an effective value over the molecular weight range we have studied in Paper I. For smaller molecular weight fractions, α_D should approach 1, while for larger molecular weight fractions, α_D should be less than 0.75. Nevertheless, over the usual range of interest for PPTA solutions using 96% H_2SO_4 as the solvent, the α_D value of 0.75 is probably a fairly good compromise. On the $G(D_0)$-axis after correction for intramolecular interference, we take

$$G(D_0)\propto M^2 F_n(M) \tag{43}$$

With $F_w(M)=MF_n(M)$, *Figure 8* shows the weight distribution of PPTA ($M_w=4.3\times 10^4$ g/mole) using independent results from two solutions at $C=2.8\times 10^{-4}$ and 5.8×10^{-4} g/ml. The analysis for the PPTA solution at $C=2.8\times 10^{-4}$ g/ml has been presented in detail as shown by *Figures 1–7*. For a separately prepared PPTA solution at $C=5.8\times 10^{-4}$ g/ml, we follow the same procedure and present only its final result as shown in *Figure 8*. The agreement between the two preparations following the same procedure is remarkable. In examining *Figure 8* closely, we have noted several surprises.

(1) The molecular weight distribution is not as broad as we originally anticipated. $M_z:M_w:M_n\simeq 6.1:1.8:1$. In making the molecular weight transform, we have taken $D_0=k_D M^{-0.75}$ and adjusted k_D $(=2.07\times 10^{-5})$ so as to make the computed M_w equal to $M_w=4.26\times 10^4$ g/mole, the value determined by light scattering intensity measurements. As $D_0=2.11\times 10^{-5}\,M_w^{-0.75}$ cm^2 s^{-1} with M_w expressed in g/mole for PPTA dissolved in 96% H_2SO_4, the adjustment in k_D corresponds to $(4.26/4.83)^{0.75}2.11\times 10^{-5}\sim 1.94\times 10^{-5}$, a 7% decrease.

Thus, the molecular weight transform uses an empirical relation which is consistent with intrinsic viscosity results and with cumulants analysis for D_z. We have also taken $\alpha_D(=0.75)$ for PPTA in 96% H_2SO_4 + MK_2SO_4 to be the same as that in 96% H_2SO_4. *Figure 6* seems to suggest that ρ is somewhat higher in the absence of salt. Then, *MWD* would have been slightly broader.

(2) The molecular weight distribution has a high molecular weight tail. While it is possible that small amounts of aggregation can produce a long tail since our Laplace inversion technique may not be able to resolve a small bump at the high molecular weight end of the molecular weight distribution, we shall formulate the problem slightly differently, i.e., given the solution, can the high molecular weight tail be produced as an artifact of our Laplace inversion technique? In this respect, we should also be interested to know the low molecular weight limit of the molecular weight distribution. In *Figure 1c*, it is the lower Γ region which produces the high molecular weight tail. *Figure 9* shows a re-analysis of $G(\Gamma)$ by arbitrarily changing upper and lower limits, Γ_{min} and Γ_{max}. It appears that the tail in the high molecular weight region falls within the uncertainties of the errors in the baseline. In order to obtain a true indication of the extent of the molecular weight distribution we have found an integrated plot, *Figure 10*, to show very clearly that the highest molecular weight fractions do not extend beyond 10^5 g/mole. Integrated weight fractions of PPTA having molecular weights greater than 5×10^5 g/mole are less than $\lesssim 1\%$ of total weight. This high molecular weight tail will become somewhat longer if α_D becomes less than 0.75 with increasing molecular weight.

Figure 11 shows a comparison of the molecular weight distribution obtained using the two different methods of time correlation function profile analysis described in the paper.

CONCLUSIONS

We have succeeded in characterizing PPTA in concentrated sulphuric acid. By combining static and dynamic properties of PPTA and the use of appropriate Laplace inversion techniques, we were able to determine, for the first time, the molecular weight distribution of PPTA. The laser light scattering technique offers a new analytical approach to size exclusion chromatography which is difficult to perform for polymer solutions in corrosive solvents.

Once we have established the effects of interference and of concentration, it is no longer necessary to perform the detailed analysis which we have presented. We need only to make one time correlation function measurement at one fixed concentration and one scattering angle, and to correct for the effects of concentration and of interference before performing the Laplace inversion and molecular weight transform. *Figure 12* shows the scaling of concentration effect at constant scattering angle. *Figure 13* shows

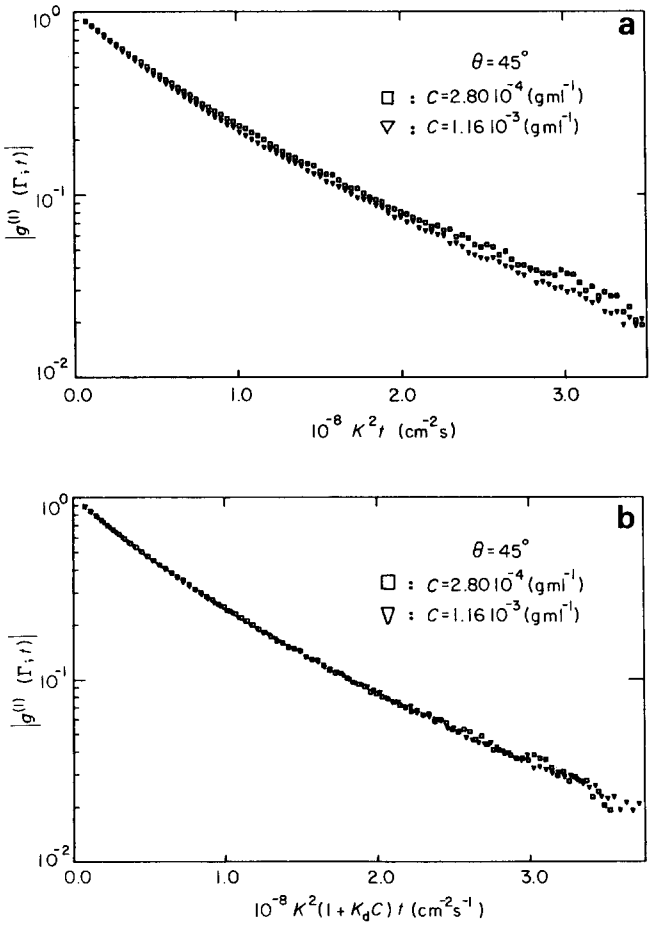

Figure 12 Scaling of $|g^{(1)}(\Gamma,t)|$ due to concentration effect at constant θ (=45°) $t=\tau$ (a) before scaling; (b) after scaling; $k_d = 60$ ml/g

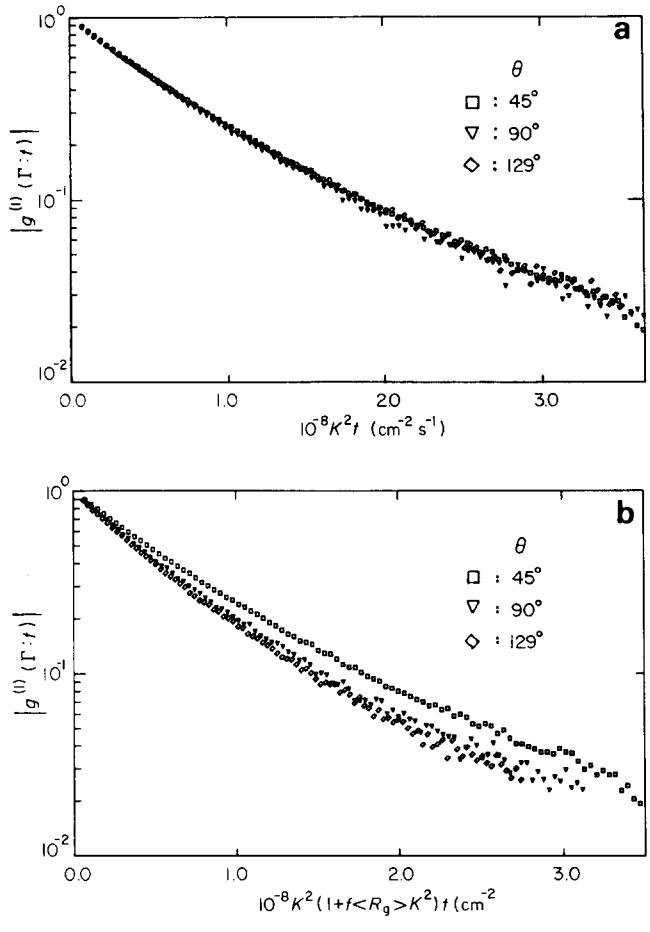

Figure 13 Scaling of $|g^{(1)}(\Gamma,t)|$ due to interference effect at constant concentration ($C = 2.80 \times 10^{-4}$ g/ml). $t=\tau$: (a) before scaling; (b) after scaling; $f\langle R_g^2\rangle$ denotes $f\langle R_g^2\rangle_{app}$ with f and R_{ga}^2 being 0.2 and 1.2×10^{-11} cm^2, respectively. □: $\theta = 45°$, $K = 1.41 \times 10^5$ cm^{-1}; ▽: $\theta = 90°$, $K = 2.60 \times 10^5$ cm^{-1}; ◇: $\theta = 129°$, $K = 3.32 \times 10^5$ cm^{-1}

the scaling of interference effect at constant concentration. The close overlap of correlation functions clearly illustrates that we can compensate for such effects based on known experimental data which are essentially constant in a given polymer system. Furthermore, as $G(\Gamma)$ is related to the shape of $|g^{(1)}(\tau)|$, we can examine shifts of sizes and its variance by examining the changes in $|g^{(1)}(\tau)|$ without the use of Laplace inversion algorithms. Thus, laser light scattering can be developed and used as monitors for polymer characteristic changes in solution, for polymers such as PPTA.

ACKNOWLEDGEMENT

We gratefully acknowledge support of this research by the National Science Foundation, Polymers Program (DMR 8314193), INT 8211992 and the Petroleum Research Fund administered by the American Chemical Society.

REFERENCES

1 Chu, B., Gulari, E. and Gulari, E. *Physica Scripta* 1979, **19**, 476
2 McWhirter, J. G. and Pike, E. R. *J. Phys. A* 1978, **11**, 1729
3 Ostrowski, N., Sornette, D., Parker, P. and Pike, E. R. *Optica Acta* 1981, **28**, 1059
4 Pike, E. R. in 'Scattering Techniques Applied to Supramolecular and Non-Equilibrium Systems' (Eds. S. H. Chen, B. Chu and R. Nossal), Plenum Press, New York (1981), p. 179
5 Bertero, M., Boccacci, P. and Pike, E. R. *Proc. Roy. Soc. Lond., A* 1982, **383**, 15
6 Stock, G. B. *Biophys. J.* 1976, **16**, 355; 1978, **18**, 79
7 Provencher, S. W. *Biophys. J.* 1976, **16**, 27; *J. Chem. Phys.* 1976, **64**, 2772; *Makromol. Chem.* 1979, **180**, 201
8 Provencher, S. W., Hendrix, J., DeMaeyer, L. and Paulussen, N. *J. Chem. Phys.* 1978, **69**, 4273
9 Ford, J. R. and Chu, B. in 'Proceedings of the 5th International Conference on Photon Correlation Techniques in Fluid Mechanics', Springer Series in Optical Sciences (Ed. E. O. Schulz-DuBois), Springer-Verlag, NY (1983), p. 303
10 See for example 'Essentials of Size Distribution Measurement', *in* 'Measurement of Suspended Particles by Quasi-Elastic Light Scattering' (Ed. B. E. Dahneke), John Wiley & Sons, N.Y. (1983), p. 81
11 See for example 'Photon Correlation Spectroscopy of Brownian Motion: Polydispersity Analysis and Studies of Particle Dynamics', *in* 'Proceedings of the 5th International Conference on Photon Correlation Techniques in Fluid Mechanics', Springer Series in Optical Sciences (Ed. E. O. Schulz-DuBois), Springer-Verlag, N.Y. (1983), p. 286; 315
12 Bertero, M., Boccacci, P. and Pike, E. R. *Proc. Roy. Soc. A* 1982, **383**, 15
13 Golub, G. H. and Reinsch, C. *Numer. Math.* 1970, **14**, 403
14 Hanson, R. J. *SIAM J. Numer. Anal.* 1971, **8**, 616
15 Lawson, C. L. and Hanson, R. J. 'Solving Least Squares Problems', Prentice-Hall, New Jersey, 1874
16 Provencher, S. W. in 'Proceedings of the 5th International Conference on Photon Correlation Techniques in Fluid Mechanics', Springer Series in Optical Sciences (Ed. E. O. Schulz-DuBois), Springer-Verlag, N.Y. 1983, p. 322
17 Chu, B., Ford, J. R. and Dhadwal, H. S. in Methods of Enzymology, Vol. 101, to be published
18 Miller, K. *SIAM J. Math. Anal.* 1970, **1**, 52
19 Tikhonov, A. N. and Arsenin, V. Y. 'Solutions of Ill-Posed Problems', V. H. Winston & Sons, Washington, D.C., 1977
20 Berto, M., DeMol, C. and Viano, G. A. in 'Inverse Scattering Problems in Optics, Topics in Current Physics (Ed. H. P. Baltes), Vol. 20, Springer-Verlag, 1980
21 Bertero, M., Viano, G. A. and DeMol, C. *Optica Acta* 1980, **27**, 307
22 Nashed, M. Z. *I.E.E.E. Trans. Antennas Propag.* 1981, **29**, 220
23 Abbiss, J. B., DeMol, C. and Dhadwal, H. S. *Optica Acta* 1983, **30**, 107
24 Groetsch, C. W. 'Generalized Inverses of Linear Operators', Marcel Dekker, Inc., New York, 1977
25 Hutson, V. and Pym, J. S. 'Applications of Functional Analysis and Operator Theory', Academic Press, New York, 1980
26 Stockmayer, W. H. and Schmidt, M. *Pure Appl. Chem.* 1982, **54**, 407
27 Schmidt, M. and Stockmayer, W. H. *Macromolecules* 1984, **17**, 509